Journal of Controlled Release 171 (2013) 184–192

Contents lists available at ScienceDirect

Journal of Controlled Release

journal homepage: www.elsevier.com/locate/jconrel

Drug-loaded sickle cells programmed *ex vivo* for delayed hemolysis target hypoxic tumor microvessels and augment tumor drug delivery ☆

Se-woon Choe [a], David S. Terman [b], Angela E. Rivers [c], Jose Rivera [d], Richard Lottenberg [e], Brian S. Sorg [f,*]

[a] Gumi Electronics & Information Technology Research Institute, Gumi, Republic of Korea
[b] Molecular Genetics Program, Jenomic Research Institute, Carmel, CA, USA
[c] Division of Pediatric Hematology/Oncology, College of Medicine, University of Illinois, Chicago, IL, USA
[d] Department of Bioengineering, University of Illinois, Urbana–Champaign, IL, USA
[e] Division of Hematology/Oncology, College of Medicine, University of Florida, Gainesville, FL, USA
[f] National Cancer Institute, National Institutes of Health, Bethesda, MD, USA

ARTICLE INFO

Article history:
Received 11 February 2013
Accepted 2 July 2013
Available online 18 July 2013

Keywords:
Blood
Cancer
Carrier
Chemotherapy
Particle
Photosensitizer

ABSTRACT

Selective drug delivery to hypoxic tumor niches remains a significant therapeutic challenge that calls for new conceptual approaches. Sickle red blood cells (SSRBCs) have shown an ability to target such hypoxic niches and induce tumoricidal effects when used together with exogenous pro-oxidants. Here we determine whether the delivery of a model therapeutic encapsulated in murine SSRBCs can be enhanced by *ex vivo* photosensitization under conditions that delay autohemolysis to a time that coincides with maximal localization of SSRBCs in a hypoxic tumor. Hyperspectral imaging of 4T1 carcinomas shows oxygen saturation levels <10% in a large fraction (commonly 50% or more) of the tumor. Using video microscopy of dorsal skin window chambers implanted with 4T1 tumors, we demonstrate that allogeneic SSRBCs, but not normal RBCs (nRBCs), selectively accumulate in hypoxic 4T1 tumors between 12 and 24 h after systemic administration. We further show that *ex vivo* photo-oxidation can program SSRBCs to postpone hemolysis/release of a model therapeutic to a point that coincides with their maximum sequestration in hypoxic tumor microvessels. Under these conditions, drug-loaded photosensitized SSRBCs show a 3–4 fold greater drug delivery to tumors compared to non-photosensitized SSRBCs, drug-loaded photosensitized nRBCs, and free drug. These results demonstrate that photo-oxidized SSRBCs, but not photo-oxidized nRBCs, sequester and hemolyze in hypoxic tumors and release substantially more drug than photo-oxidized nRBCs and non-photo-oxidized SSRBCs. Photo-oxidation of drug-loaded SSRBCs thus appears to exploit the unique tumor targeting and carrier properties of SSRBCs to optimize drug delivery to hypoxic tumors. Such programmed and drug-loaded SSRBCs therefore represent a novel and useful tool for augmenting drug delivery to hypoxic solid tumors.

Published by Elsevier B.V.

1. Introduction

Hypoxic tumor niches are present in the vast majority of human solid cancers and constitute a major cause of therapeutic resistance and tumor recurrence. Treatment failure of such hypoxic tumors is largely attributable to the nature of the tumor microenvironment whose neovasculature is poorly perfused leading to impaired drug transport and low tumor cell drug concentrations [1]. Previous studies have shown that sickle red blood cells (SSRBCs) but not normal RBCs (nRBCs) possess the unique ability to selectively target such hypoxic solid tumors wherein they form microaggregates, occlude tumor microvessels, and release intrinsic pro-oxidants that contribute to the tumoricidal response[2,3]. The unique ability of activated SSRBCs, but not normal RBCs (nRBCs), to target and occlude tumor microvasculature is based in part on their expression of multiple adhesion receptors which bind cognate ligands expressed in tumor microvessels in response to hypoxic conditions [2,4].

Since SSRBCs are capable of accessing poorly perfused hypoxic tumors, we reasoned that their tumoricidal effect could be increased if they were loaded with a therapeutic cargo that could be co-released with their intrinsic pro-oxidants into the tumor parenchyma. We contemplated further enhancement of the therapeutic effect if release of loaded drug from the SSRBCs could be controlled and timed to coincide with maximum sequestration of SSRBCs in the tumor. In this context, we turned to a system of *ex vivo* photo-oxidation [5–7] and established conditions that would delay maximum hemolysis of drug-loaded SSRBCs *in vivo* to coincide with deposition of the vast majority of allogeneic SSRBCs in the tumor.

☆ The opinions expressed in this article are the authors' own and do not reflect the view of the National Institutes of Health, the Department of Health and Human Services, or the United States government.

* Corresponding author at: Cancer Diagnosis Program, Division of Cancer Treatment and Diagnosis, National Cancer Institute, 9609 Medical Center Dr., Bethesda, MD 20892, USA. Tel.: +1 240 276 5712.
E-mail address: brian.sorg@nih.gov (B.S. Sorg).

0168-3659/$ – see front matter. Published by Elsevier B.V.
http://dx.doi.org/10.1016/j.jconrel.2013.07.008

In this study, we show that SSRBCs, loaded with a model drug, can be programmed by *ex vivo* photo-oxidation to undergo maximum hemolysis *in vivo* at a point that corresponds to their maximal sequestration in hypoxic tumor blood vessels. Under such conditions, these SSRBCs can deliver a significantly larger fraction of drug to tumors relative to non-photo-oxidized SSRBCs, drug loaded photo-oxidized nRBCs, and free drug.

2. Materials and methods

All experiments were conducted in accordance with protocols approved by the University of Florida Institutional Animal Care and Use Committee.

2.1. Tumor-bearing mice and mouse models of sickle cell disease

Female athymic nude mice of about 25 g weight were used as tumor-bearing animals. Two different transgenic mouse models of sickle cell disease were used to provide blood for experiments: the Berkeley mouse, one of the most commonly used sickle cell rodent models [8,9] and the Knock-in mouse (B6;129-Hba$^{tm1(HBA)Tow}$ Hbb$^{tm2(HBG1,HBB*)Tow}$/Hbb$^{tm3(HBG1,HBB)Tow}$/J), a recently developed model considered superior to the Berkeley mouse [10,11]. C57BL/6 mice, the background mice for the disease models, were used for control wild-type blood (nRBCs).

2.2. Window chamber installation

Female athymic (nu/nu) nude mice (Harlan Laboratories) were surgically implanted with titanium dorsal skinfold window chambers while under anesthesia (ketamine, 100 mg/kg and xylazine, 10 mg/kg, i.p.). During surgery one layer of dorsal skin was removed in a circular area of about 12 mm diameter and covered with a glass coverslip. A window chamber tumor was established during chamber implantation by injecting 10 μL of a single cell suspension (10×10^3cells in serum-free media) of 4T1 mouse mammary adenocarcinoma tumor cells into the dorsal skin flap prior to placing a 12 mm diameter #2 round glass coverslip over the exposed skin. The tumor cells were a gift from Mark W. Dewhirst (Duke University, Durham, NC). After recovery from surgery, animals were housed in an environmental chamber maintained at 33 °C and 50% humidity with free access to food and water and standard 12 hour light/dark cycles.

2.3. Hemoglobin saturation imaging

Hemoglobin saturation measurements of tumor microvasculature were accomplished *via* spectral imaging microscopy of window chamber tumors. The image acquisition and processing methods were discussed in detail previously [12,13]. Briefly, a Zeiss microscope (Carl Zeiss, Incorporated, Thornwood, NY) was used as the imaging platform, and band-limited images of trans-illuminated window chambers were acquired using a liquid crystal tunable filter (CRI, Inc., Woburn, MA) placed in front of a monochrome scientific grade CCD camera thermoelectrically cooled to −20 °C (DVC Company, Austin, TX). Microvessel hemoglobin saturation measurements and images were created from the spectral image data based on reference spectra of pure oxy- and deoxyhemoglobin.

2.4. SSRBC in vivo tumor accumulation measurements

2.4.1. Labeling of blood cells

RBCs from donor patients and mice were fluorescently labeled with a 1 mM stock solution of the carbocyanine dye 1,1′-dioctadecyl-3,3,3′,3′-tetramethylindodicarbocyanine, 4-chlorobenzenesulfonate salt (DiD, D-7757 from Invitrogen, Carlsbad, CA) in ethanol using a modified procedure by Unthank et al. [14]. Briefly, the RBCs were prepared for labeling by centrifugation at 4 °C and resuspension in Dulbecco's Phosphate Buffered Saline (DPBS) without phenol red (HyClone Laboratories, Logan, UT) and with 1 mM of Ca^{2+} and 0.5 mM of Mg^{2+} added to the buffer. The RBCs were repeatedly centrifuged and resuspended until the supernatant was clear. A 200 μL aliquot of packed cells was incubated with 200 μL of DiD stock solution in 10 mL of sterile DPBS at room temperature for 30 min. The samples were covered with aluminum foil during handling to protect the samples from ambient light. Unbound DiD dye was removed by repeated washing steps with DPBS.

DiD-labeled RBCs in 200 μL of DPBS (hematocrit of 50%) were administered by tail vein injection when the window chamber tumors reached a diameter of about 6 mm. The quantity of administered RBCs did not exceed 12% of the total circulating amount assuming that the mouse blood volume was 1.7 mL, thereby minimizing rheologic effects attributable to increased hematocrit [15].

2.4.2. In vivo microscopy and analysis

A Zeiss microscope (Carl Zeiss, Incorporated, Thornwood, NY) was used as the imaging platform. A 100 W tungsten halogen lamp was used for transillumination of the window chamber while a mercury lamp provided epi-illumination for fluorescence imaging. Brightfield transmitted light images were acquired with a monochrome scientific grade CCD camera thermoelectrically cooled to −20 °C (DVC Company, Austin, TX) and fluorescence images were acquired with an ANDOR iXon electron multiplying CCD (EMCCD) camera thermoelectrically cooled to −50 °C (ANDOR Technology, South Windsor, CT). Mice were anesthetized for imaging with 1–2% isoflurane in air and body temperature was maintained with a temperature-controlled small animal heating pad (World Precision Instruments, Sarasota, FL). At least 6 regions-of-interest (ROIs) were randomly imaged per mouse for both tumor areas and adjacent normal tissue areas, and at least 6 mice were used per group. Single images were acquired at various time points up to 12 h after administration of labeled RBCs. Fast-moving non-stationary fluorescent RBCs appeared as a blurred background with increased image exposure times of around 150 ms, while motionless fluorescent RBCs were easily observed due to their brighter point-like fluorescence signal. Bright spots were counted as accumulated cells and quantified by image processing using MATLAB software (The MathWorks, Incorporated, Natick, Massachusetts) as was done previously [16]. In an additional analysis method, fluorescently labeled RBCs were recorded *via* streaming video analysis. A total of 1500 frames of streaming video with frame exposure times of 200 ms were acquired for 5 minute durations at 0, 30, 60, 90, 180, 360 and 720 min after administration of labeled RBCs. Fluorescent cells that appeared to be immobile for over 1 continuous minute of observation were considered to be accumulated cells and counted manually.

2.4.3. Histological analysis

Liver, spleen, and the 4T1 window chamber tumor were harvested immediately after the imaging session at 12 h post-administration of labeled RBCs. The harvested tissues were fixed with 10% formalin, dehydrated with 15%–30% sucrose solution, embedded in optimal cutting temperature (OCT) solution (Tissue-Tec OCT, Fisher Scientific, Pittsburgh, PA) in plastic cryomolds, and snap-frozen above dry ice in methylbutane at about −55 °C. Specimens were sectioned at 20 μm by microtome (Microm, HM550 microtome/cryostat, Microm International, Walldorf, Germany) at −18 °C. The slides were air dried at room temperature overnight. Unstained slides were examined for fluorescence from labeled RBCs using five random fields at 20× magnification on each of two consecutive sections for each tissue sample. The fluorescence signal from labeled RBCs in each field was measured, and the average for all measured fields was computed as the value for that specimen.

2.5. RBC hypotonic pre-swelling loading

Calcein is a fluorescent dye commonly used in drug carrier controlled release studies as it is self-quenching in high concentrations

inside carriers, but fluoresces upon release [17,18]. Calcein served as the model payload in this study. The hypotonic pre-swelling method, one of several osmosis-based red blood cell loading methods [19], was used in a modified form for loading of calcein. Exposing RBCs to a hypotonic solution leads to an enhanced permeability of the membrane due to creation of pores with diameters of ~20–50 nm in the membrane [20]. RBCs in 1 mL of DPBS solution were repeatedly washed *via* centrifugation at 4 °C and resuspended in DPBS until the supernatant was clear. Packed cells were placed in polypropylene tubes in 200 μL aliquots and 1.2 mL of hypotonic DPBS solution with an osmolarity of 0.67 was added into each tube. The cell suspension was gently mixed for 5 min and then centrifugated at 4 °C to separate swollen cells. The supernatant was discarded and a 40 μL of aliquot of hemolysate derived from lysed cells (RBCs:DIH_2O at 1:1 [v:v]) was carefully added above the swollen cells to compensate for loss of intracellular components during the loading procedure. The addition of the hemolysate solution also helped reduce the osmolarity shock to the swollen cells when the aqueous dye solution was added. After addition of hemolysate, 250 μL of an aqueous hypotonic solution of calcein (77.8 μg/mL) or cisplatin (150 μg/mL) was carefully added in each tube and mixed for 5 min. When the transparency of the supernatant was suddenly increased and white ghost cells were observed at the boundary between the supernatant and packed cells, the hemolysis point of the RBCs was achieved. At this point, 100 μL of hypertonic solution (10 × PBS) was added rapidly in each tube to reseal the pores created during cell swelling. Cell suspensions were gently mixed for 5 min and incubated at 37 °C for 30 min to reanneal and reseal the cells. The RBCs were washed twice in DPBS to remove unloaded calcein and resuspended to give an approximate concentration of 8×10^8 cells/mL for experiments.

2.6. Delayed photolysis in vitro measurements

2.6.1. Photosensitization of RBCs

RBCs in 1 mL of DPBS were washed by repeated centrifugation at 4 °C and resuspension in DPBS (the supernatant was discarded). For the final wash the supernatant was discarded and the cells were left in a concentrated state. The concentrated cells were incubated with 6 mL of protoporphyrin IX (PpIX) at various concentrations in DPBS at 37 °C for 30 min. The RBCs were manually mixed by gentle swirling once during the incubation period. After incubation, the cells were washed twice in DPBS by centrifugation and resuspension to remove unbound photosensitizer. The final resuspension was in 3 mL DPBS solution, and the treated cells were stored at 4 °C until use. To protect the photosensitized RBCs from ambient light, the sample preparation tubes were covered by aluminum foil during all procedures.

2.6.2. Delayed photolysis and calcein release measurements

Photosensitized RBCs were transferred to a 3 mL glass cuvette placed in a temperature controlled cuvette holder (Quantum Northwest, Inc., Liberty Lake, WA). The solution in the cuvette was irradiated by a halogen lamp at 0.08 W or 0.33 W at 24 °C for various time durations to initiate the photochemical reaction. After light activation, the halogen lamp was switched off and the sample was heated to physiological temperature (37 °C) in the dark. The delayed photolysis rate was measured from the beginning of the dark incubation period.

Delayed photolysis of RBCs was measured *in vitro* using hemoglobin release from unmodified cells and calcein release from cells loaded by hypotonic pre-swelling loading. For hemoglobin release, small samples (30 μL) were withdrawn periodically from the test solution for lysis measurements. The collected sample was immediately centrifuged and 20 μL of supernatant was saved for analysis. The hemoglobin released into solution by photolysis was determined by spectrophotometric absorbance measurement at 415 nm on a NanoDrop 1000 spectrophotometer (Thermo Fisher Scientific, Wilmington, DE). The fractional photolysis was determined from the absorbance of a collected sample normalized to the absorbance of a sample from an equivalent solution of fully lysed cells. nRBCs and SSRBCs were handled and treated identically for delayed photolysis measurements. For calcein release, calcein fluorescence was measured spectrophotometrically at 520 nm using a microplate reader (BioTek Synergy HT, BioTek, Winooski, VT), while for cisplatin release, inductively coupled plasma-atomic emission spectrometry (ICP-AES) was used for platinum (Pt) measurement (Optima 3200 RL, PerkinElmer, Boston, MA) similar to methods published in the literature [21]. A standard calibration curve was created from samples of cisplatin at different concentrations in DPBS buffer so that a consistent loading concentration (approximately 10.5 ppm) could be achieved in the RBCs. Cisplatin release rates were made relative to completely lysed batch samples similar to the calcein measurements.

A Gompertz equation was fit to the data in some cases to calculate the t_{50} release time (time for 50% release of contents) as previously reported research showed that RBC photolysis follows a Gompertz curve [22].

2.7. Delayed photolysis in vivo measurements

Single cell suspensions of 1×10^5 4T1 cells in 100 μL DMEM without serum were injected subcutaneously over the left quadriceps muscle of anesthetized (1–2% isoflurane) female athymic nude mouse. After the tumor cell injection, mice were housed with free access to food and water and standard 12 hour light/dark cycles. *In vivo* delayed photolysis measurements were performed when tumors reached ~10 mm diameter.

Mice were randomly assigned to one of four different groups ($n = 5$ each group): (1) free calcein, (2) calcein-loaded SSRBCs with photoactivation, (3) calcein-loaded SSRBCs without photoactivation, and (4) calcein-loaded nRBCs with photoactivation. The calcein dose for each group was 40 mg/kg administered *via* tail vein injection. In the calcein-loaded nRBC and SSRBC groups, a 200 μL bolus of 50% v/v calcein-loaded cells was used. Calcein-loaded RBCs were photosensitized with 25 μM PpIX and photoactivated *ex vivo* by 0.08 W halogen lamp for 1 min at 24 °C immediately prior to systemic administration (one SSRBC group did not receive photoactivation as previously noted).

Calcein deposition in the flank tumors was measured at 12, 24, and 48 h after RBC or free calcein administration using microdialysis (48 hour time point for photoactivated SSRBC group only). A microdialysis probe with a 20 kDa membrane cut-off (CMA microdialysis, Kista, Sweden) was placed in the tumor ~5 mm below the tumor surface through a small scalpel incision. Another probe was placed in the quadriceps muscle of the opposite leg in the same animal as a control reference site. Microdialysis probes were perfused with Ringer's solution at a flow rate of 1 μL/min. After a 30 min equilibration period, dialysate samples were collected from the tumor and quadriceps muscle over a 4 hour interval using a probe perfusion rate of 1 μL/min for a total collected microdialysate volume of 240 μL at the time points. The fluorescence signal of calcein in the dialysate was measured in a microplate reader (BioTek Synergy HT microplate reader, BioTek, Winooski, VT).

Statistical analysis of all data in this study was performed using SPSS software (SPSS for Windows; SPSS Inc., Chicago, IL). Analysis of variance (ANOVA) followed by Bonferroni's post hoc test were used to compare the data with $p < 0.05$ level of statistical significance.

3. Results

The murine models of sickle cell anemia are now regarded as excellent replicas of the human SS disease [11,23]. Thus, we used both Townes (Knock-in) and Berkeley SS disease models for the foregoing studies. Fig. 1 shows accumulation of exogenously administered SSRBCs, from the mouse models of sickle cell disease, in 4T1 tumors grown in athymic nude mice. Fig. 1A shows a quantitative ROI analysis of fluorescence from tumor regions normalized to fluorescence from adjacent normal tissue ROIs at 12 h after systemic administration of SSRBCs from Knock-in and Berkeley mice. Preferential tumor accumulation of SSRBCs

is demonstrated, and such accumulation is not seen with nRBCs from C57BL/6 wild-type mice. In Fig. 1B is an alternate analysis of SSRBC accumulation in tumors using video microscopy. Flowing fluorescent labeled erythrocytes that were observed to stop and remain immobile for at least 1 min during a 5 minute observation period were counted as accumulated cells. In Fig. 1B is the number of immobilized red blood cells in tumor regions normalized to that in adjacent normal tissue at 12 h after systemic administration of red blood cells. The graph in Fig. 1B shows good agreement with that in Fig. 1A, demonstrating SSRBC accumulation in tumors using both analysis techniques. SSRBCs from Knock-in mice were used for subsequent experiments since these cells had more accumulation in the same time period than those from Berkeley mice.

Fig. 2 shows the histological analysis of accumulation of fluorescently labeled SSRBCs grown in 4T1 window chamber tumors compared to SSRBCs in liver and spleen at 12 h post-administration. A baseline average nRBC fluorescence signal at each location (liver, spleen, tumor) from a separate group of animals was subtracted from the SSRBC average fluorescence signal, using similarly treated SSRBCs, to account for the signal due to flowing blood. Thus the plotted signal, ΔFluorescence, should be due to SSRBCs that have accumulated and are not flowing. Significantly more SSRBCs ($p < 0.05$) accumulated in the tumor (≥4.75× fluorescence signal in tumor) compared to liver and spleen.

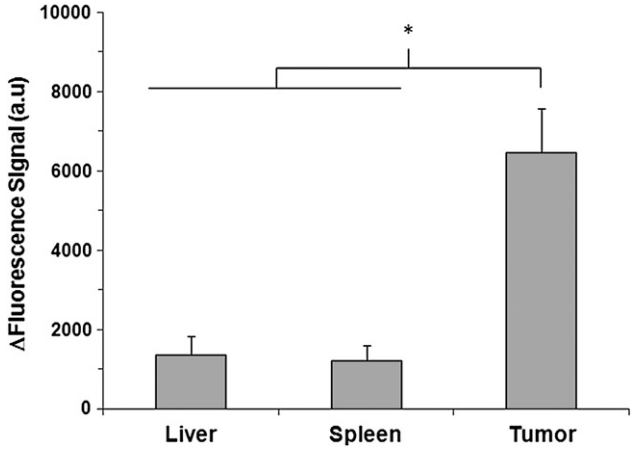

Fig. 2. Histological analysis of SSRBC accumulation in the liver (n = 6), spleen (n = 8), and 4T1 tumors (n = 17). Measurement of the difference in fluorescence signal (ΔFluorescence, arbitrary units) from labeled wild-type RBCs from C57BL/6 mice and SSRBCs from Knock-in mice show enhanced accumulation of SSRBCs in the tumor (≥4.75× fluorescence signal of liver and spleen). Values are given as mean ± standard deviation and * = $p < 0.05$ (ANOVA followed by Bonferroni's post-hoc test).

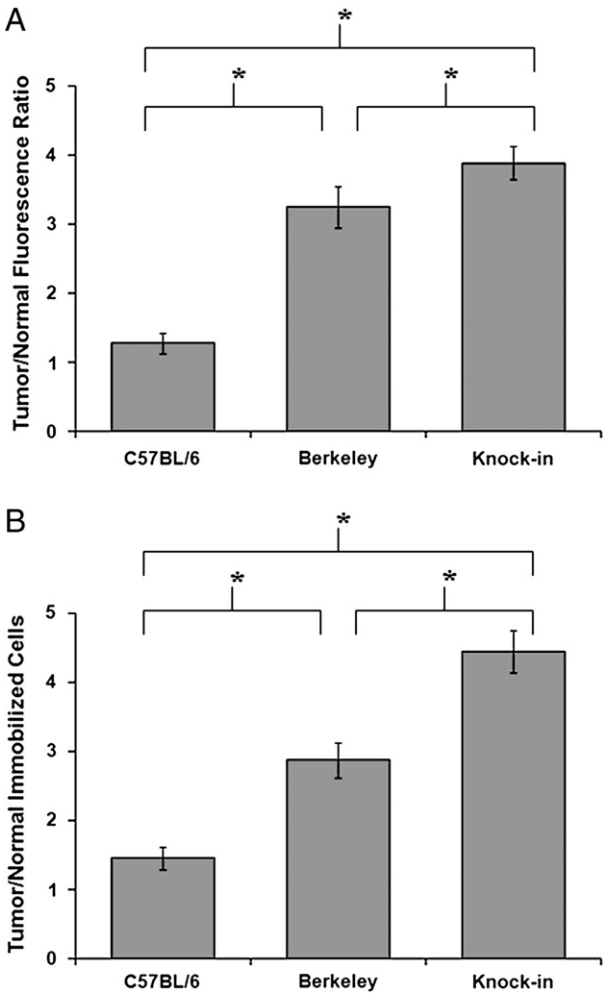

Fig. 1. Accumulation of sickle cells in 4T1 mouse mammary adenocarcinomas grown in dorsal skin window chambers. (A) Fluorescence from tumor regions normalized to adjacent tissue regions 12 h after systemic administration of erythrocytes (mean ± standard deviation, * = $p < 0.05$, ANOVA followed by Bonferroni's post-hoc test). (B) Number of immobile cells from tumor regions normalized to adjacent tissue regions for video analysis method 12 h after systemic administration of erythrocytes (mean ± standard deviation, * = $p < 0.05$, ANOVA followed by Bonferroni's post-hoc test).

Fig. 3 shows that the typical 4T1 window chamber tumor 11 days after tumor cell implantation has regions of low tumor oxygenation

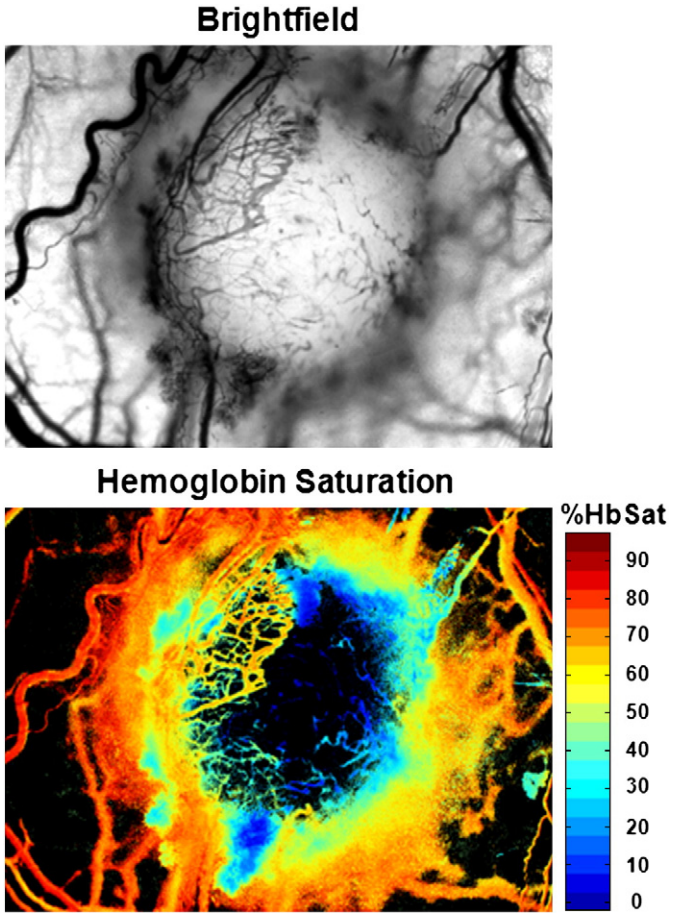

Fig. 3. Brightfield and hemoglobin saturation images of a 4T1 tumor 11 days after implantation in a mouse dorsal skin-fold window chamber. The colorbar to the right of the hemoglobin saturation image indicates the percent hemoglobin saturation of the corresponding pixels. The image field-of-view is about 3.6 mm high × 4.9 mm wide.

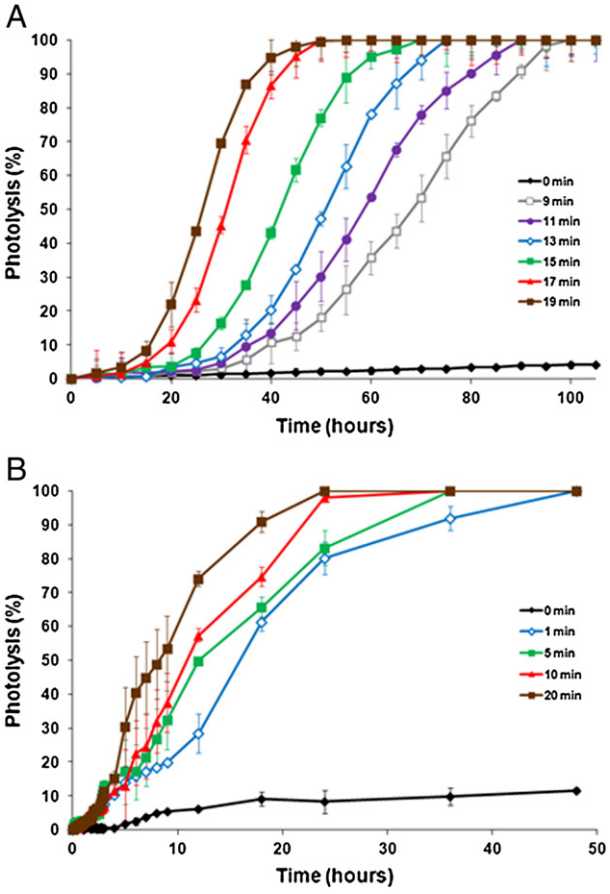

Fig. 4. *In vitro* delayed photolysis of mouse red blood cells. Hemoglobin release was measured by optical absorption spectroscopy at 415 nm to track the rate of photolysis. The data points show the percent photolysis (mean ± standard deviation). (A) Delayed photolysis of wild-type C57BL/6 red blood cells. The red blood cells were photosensitized by incubation with 50 μM PpIX, and photoactivation was by halogen lamp for the times indicated at 0.33 W in a 24 °C degree solution with dark incubation at 37 °C. Control samples were not photosensitized or irradiated. Delayed photolysis was measured from the start of dark incubation. (B) Delayed photolysis of sickle cells from Knock-in mice. The sickle cells were photosensitized by incubation with 25 μM PpIX, and photoactivation was by halogen lamp for the times indicated at 0.08 W in a 24 °C degree solution with dark incubation at 37 °C.

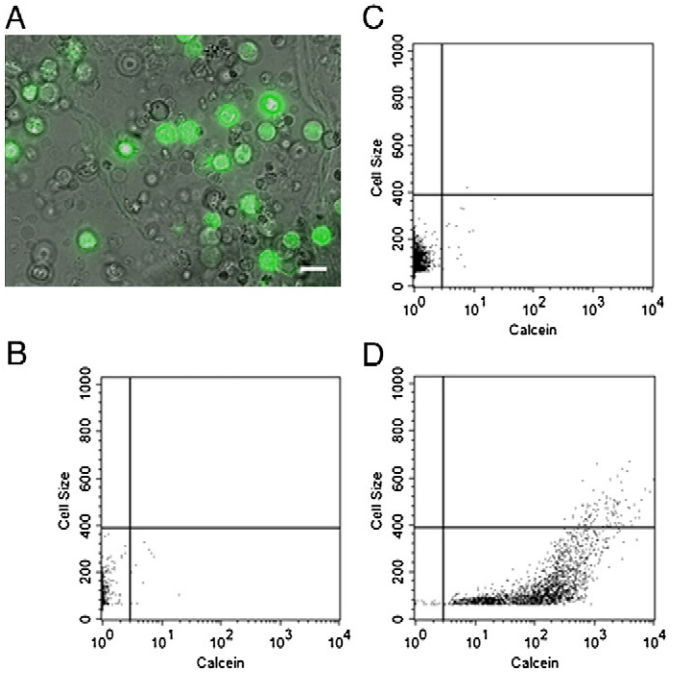

Fig. 5. Optical microscopy and flow cytometry analysis of calcein loading of sickle cells from Knock-in mice. (A) Image of calcein fluorescence from loaded sickle cells overlaid on the corresponding transmitted light image. (B) Flow cytometry data of unloaded (native sickle cells). Calcein fluorescence is plotted on the abscissa and cell size estimate from scattering is plotted on the ordinate. (C) Flow cytometry data of sham loaded sickle cells. (D) Flow cytometry data of calcein loaded sickle cells.

that are clearly evident and identified by the low hemoglobin saturation values in the tumor microvasculature.

Fig. 4 shows initial *in vitro* delayed photolysis experiments in which the release of hemoglobin from RBCs was measured. Photoactivation was by halogen lamp of a red blood cell solution at 24 °C followed by incubation in the dark at 37 °C. Delayed photolysis was measured from the start of dark incubation. In all cases, control samples were not photosensitized or irradiated. In Fig. 4A, wild-type red blood cells from C57BL/6 mice were photosensitized with 50 μM PpIX and irradiated for 9–19 min at 0.33 W incident power. In Fig. 4B, SSRBCs from Knock-in mice were photosensitized with 25 μM PpIX and irradiated for 1–20 min at 0.08 W incident power. Pilot experiments showed that the SSRBCs had similar photolysis release rates as wild-type C57BL/6 red blood cells for the same photolysis activation parameters of photosensitizer concentration and light activation. The data in Fig. 4A demonstrate control over the delayed photolysis rate by varying the irradiation time, similar to previously published reports [5,6,22]. However, based on the tumor accumulation data of SSRBCs in Fig. 2, these release rates were deemed to be too fast for effective preferential *in vivo* delivery of cargo to tumors. Therefore, in Fig. 4B for the SSRBCs less photosensitizer was used and the light dose was decreased (less irradiation power and shorter irradiation times). The stringent control over the delayed photolysis release rate, obtained by varying the light dose *via* changes in irradiation time, seen in Fig. 4A was difficult to achieve for the longer release rates in Fig. 4B. However, the release rates on the order of many hours obtained in Fig. 4B were expected to be useful for preferential delivery of cargo to tumors by delayed photolysis of SSRBCs.

The release curves have the expected sigmoidal shape, and thus can be modeled mathematically by families of sigmoid curves [22]. Table 1 contains data corresponding to 50% release times (t_{50}) derived from the empirical data and from a fit of a Gompertz equation to the data in Fig. 4B. For these photoactivation conditions, it can be seen that 50% release times of about 8–16 h were achieved while non-activated control samples at 24 h only showed about 10% release by passive mechanisms. The longer t_{50} values in this study are consistent with others reported in the literature, although there are some important distinctions in terms of red blood cells and photosensitizer used, light activation times, and dark incubation temperatures. Valenzeno reported a t_{50} of about 30 h using healthy human red blood cells photosensitized with 1.44 μM hematoporphyrin derivative after light activation for 25 s with dark incubation at room temperature [7]. Pooler reported a t_{50} of about 30 h using healthy human red blood cells photosensitized with 30 nM phloxine B after light activation for 1 h and dark incubation at 4 °C [24]. Al-Akhras reported a t_{50} of about 11 h using healthy bovine red blood cells photosensitized with 10 μM PpIX after light activation for 3 min and dark incubation at 5 °C [22].

Table 1
Delayed photolysis 50% release times (t_{50}) for the data in Fig. 2B. Empirical data is shown as mean ± standard deviation; t_{irr} = irradiation (light activation) time.

t_{irr} (min)	t_{50} (min) empirical	t_{50} (min) Gompertz
1	940 ± 3.0	934
5	777 ± 3.4	810
10	664 ± 4.9	654
20	476 ± 8.2	477

Fig. 5 shows the results of hypotonic pre-swelling loading of calcein in SSRBCs from Knock-in mice. Imaging was used to assess morphological effects of the loading procedure on the RBCs. Flow cytometry was used to confirm morphology information from imaging and also determine loading efficiency. In Fig. 5A is an image of calcein-loaded SSRBCs. The image shows calcein fluorescence overlaid on a transmitted light image of the SSRBCs. From this image, it can be seen that the calcein loading procedure did not cause substantial sickling events in the SSRBCs. The flow cytometry data shown in Figs. 5B–D also confirms only minor morphological perturbations to the SSRBCs following hypotonic pre-swelling loading of calcein. The calcein entrapment efficiency, determined by flow cytometry measurements of the fraction of cells detected with measureable fluorescence compared to all counted cells, was about 85% which is consistent with reported loading efficiencies for this method in nRBCs [25,26].

Fig. 6 shows the results of SSRBC delivery of calcein to 4T1 flank tumors in nude mice with controlled release by delayed photolysis. Two microdialysis probes were placed in each animal during dialysate collection, one in the tumor ("Tumor") and one in the quadriceps muscle of the opposite leg ("Normal"). SSRBCs were photosensitized with 25 μM PpIX and photoactivation was performed *ex vivo* by 0.08 W halogen lamp for 1 min at 24 °C immediately prior to systemic administration *via* tail vein. From the data in Figs. 2 and 4B, it was expected that SSRBCs would substantially accumulate in the tumors between 12 and 24 h after systemic administration, and that about 50% delayed photolysis release of calcein would occur between 15 and 16 h after photoactivation and administration. Calcein delivery to tumors was measured *via* microdialysis at 12 and 24 h (and 48 h for photoactivated SSRBCs) after systemic administration of SSRBCs, and calcein deposition in quadriceps muscle in the same animal was used as a reference for normal tissue. Calcein delivery to tumors was clearly enhanced for photoactivated SSRBCs compared to non-photosensitized SSRBCs, photoactivated normal red blood cells from wild-type C57BL/6 mice, and free calcein.

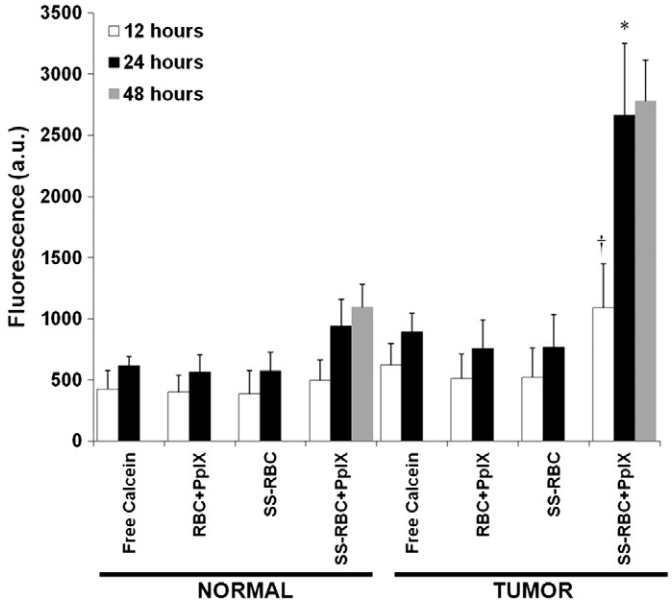

Fig. 6. Calcein delivery to tumors *in vivo* using sickle cells with *ex vivo* photoactivation for delayed photolysis controlled release. The data in the graph are the fluorescence signal from the collected microdialysis samples (mean ± standard deviation, n = 4 mice per group). Two microdialysis probes were placed in each animal during dialysate collection, one in the tumor ("Tumor") and one in the quadriceps muscle of the opposite leg ("Normal"). Photoactivated sickle cells enhance deposition of calcein in tumors relative to reference normal tissue. Calcein delivery to tumors was enhanced for photoactivated sickle cells (SS-RBC + PpIX) compared to non-photosensitized sickle cells (SS-RBC), photoactivated normal red blood cells from wild-type C57BL/6 mice (RBC + PpIX), and free calcein, with statistically greater delivery seen at 12 (†) and 24 (*) h (ANOVA followed by Bonferroni's post-hoc test, $p < 0.05$) compared to the other methods at the same time points (data at 48 h not available for the other groups).

Thus, both the tumor targeting ability of the SSRBCs and the controlled release from delayed photolysis were necessary to obtain enhancement of tumor calcein delivery. Additionally, the ability to photo-activate the carriers *ex vivo* prior to systemic administration suggests that this method may be used for controlled release to target multiple tumors simultaneously anywhere in the body, something that is beyond the capabilities of light-based methods of controlled release that require light delivery directly to the carriers inside the tumor.

While calcein is often used as a stand-in for drugs in preliminary phases of drug carrier development, the release characteristics of actual therapeutic agents can differ from calcein and must be tested individually. This concept is true for passive release from carriers as well as for delayed photolysis controlled release from carriers. An initial test of delayed photolysis release of a chemotherapeutic agent illustrates this point. We examined *in vitro* release of cisplatin from SSRBCs and compared it to calcein and hemoglobin release. Due to the highly toxic side effects of platinum-based agents, several efforts have been made to encapsulate them in carriers for improved toxicity and efficacy responses [27,28]. SSRBCs loaded with either calcein, cisplatin, or unloaded SSRBCs were sensitized with 25 μM PpIX and photoactivated with a halogen lamp for 1 min at 0.08 W similar to the data in Fig. 4B. As shown in Fig. 7, calcein release was similar to that in Fig. 4B and comparable to hemoglobin release, with 50% release occurring roughly 16–18 h after photoactivation. In contrast, cisplatin release is much faster, with 50% release occurring about 8 h after photoactivation. Given the accumulation time of the SSRBC carriers used in this study, the activation parameters for cisplatin release would likely have to be adjusted to slow the release of cisplatin in order to maximize local release in the tumors rather than in the systemic circulation.

4. Discussion

In this study we address a major therapeutic challenge, *i.e.* the treatment of hypoxic tumors that are notable for their resistance to chemotherapy and radiation. To this end, we report several novel findings as follows: First, using video microscopy of dorsal skin window chambers implanted with 4T1 tumors we demonstrate that SSRBCs show enhanced accumulation in hypoxic 4T1 tumors between 12 and 24 h after systemic administration. SSRBC accumulation in tumors also exceeded that of SSRBCs in the liver and spleen. Second, we show that *ex vivo* photo-oxidation can program drug-loaded SSRBCs, but not nRBCs, to delay hemolysis and release of a model therapeutic to

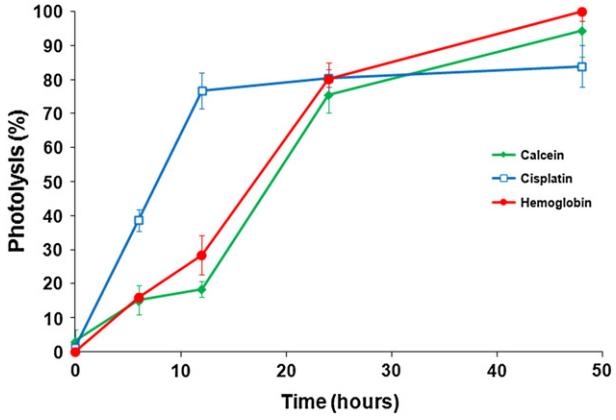

Fig. 7. *In vitro* delayed photolysis release of cisplatin from sickle cells from Knock-in mice compared to calcein and hemoglobin release. The sickle cells were photosensitized by incubation with 25 μM PpIX, and photoactivation was by halogen lamp for 1 min at 0.08 W in a 24 °C degree solution with dark incubation at 37 °C. Delayed photolysis was measured from the start of dark incubation. Hemoglobin release was measured by optical absorption spectroscopy at 415 nm, calcein release was measured using a fluorescence plate reader, and cisplatin release was measured using ICP-AES. The data points show the percent photolysis (average ± standard deviation) with n = 4 for each data point.

correspond with maximum sequestration of SSRBCs in hypoxic tumor microvessels. Third, under these conditions, photosensitized drug-loaded SSRBCs show 3–4 fold greater drug delivery to tumors compared to drug-loaded non-photosensitized SSRBCs, drug-loaded photosensitized nRBCs, and free drug. Photo-oxidation of drug-loaded SSRBCs therefore appears to exploit the tumor targeting and carrier properties of SSRBCs to optimize drug delivery and drug release in hypoxic tumors.

In Fig. 1, allogeneic SSRBCs show substantial accumulation in 4T1 tumors 12–24 h after systemic administration. Concurrently, we noted that under certain conditions 50% delayed photolysis release of calcein can be achieved between 15 and 16 h after photoactivation. As predicted from these data, SSRBCs undergo 50% hemolysis *in vivo* when they are also maximally sequestered in the tumor microvessels resulting in maximum calcein release. Calcein delivery to tumors by SSRBCs is clearly enhanced by prior photo-oxidation since non-photosensitized SSRBCs did not release more calcein in the tumor than controls. Likewise, tumor localization of SSRBCs appears to be critical to the increased calcein release since photoactivated nRBCs did not show targeted tumor deposition or significant calcein release in tumors. Importantly, compared to normoxic normal skeletal tissues, the drug-loaded and photo-oxidized SSRBCs showed enhanced drug release in tumor tissue. This suggests that the hypoxic tumor microenvironment may promote hemolysis and release drug cargo by photo-oxidized SSRBCs. To this point, SSRBCs' inherent fragility due to lipid peroxidation/thiol auto-oxidation is further promoted by hypoxia-driven auto-oxidation and S hemoglobin polymerization [29,30]. Thus, the hypoxic milieu of the 4T1 tumor may augment the natural hemolytic tendency of photo-oxidized SSRBCs and account for the increased drug release in tumors relative to normoxic skeletal muscle tissue during the measurement timeframe.

Fig. 2 shows that the drug-loaded SSRBCs localized in tumors to a significantly greater degree ($\geq$4.75×) than in the liver and spleen, sites of known SSRBC accumulation in human sickle cell anemia patients [31–33]. These findings indicate an affinity of allogeneic SSRBCs for tumor microvasculature and are consistent with earlier findings using human SSRBCs in mice [2]. The enhanced ability of SSRBCs to sequester in tumor microvasculature may be attributed in part to SSRBCs' expression of multiple adhesion receptors which bind cognate ligands in hypoxic tumor microvessels [2,4]. Ongoing investigation is addressing this point together with a biodistribution and toxicity follow-on study.

Calcein is an established model drug and widely used in cell transport studies based on its physical properties [34,35]. Like many cancer therapeutics, it is a small molecule (molecular weight ~622) and relatively hydrophilic. Since calcein is fluorescent, self-quenches at high concentrations inside of drug carriers and fluoresces upon release, it is an excellent model drug for controlled release studies [36]. For encapsulation of calcein in SSRBCs we used the classic hypotonic dialysis method which produced an 85% uptake and a calcein efflux rate that could be varied from 12 to 24 h as discussed below. As a method for the preparation of carrier erythrocytes, hypotonic dialysis or variations thereof are universally deployed because they permit incorporation of substances with diverse structures, molecular weights and physico-chemical properties without cell lysis [19,37]. The *in vitro* release of substances encapsulated in erythrocytes by this method occurs *via* first-order kinetics of diffusion through the intact cell membrane [38]. Importantly, even with technical variations to accommodate the physico-chemical properties of a candidate compound, the fundamental method induces minimal biophysical and immunological alterations and conserves the metabolic functions/energetic state of the encapsulated agent [39–41]. In implementing this method, the efflux rate of the compounds from the carrier erythrocytes *via* diffusion through the intact cell membrane ranges from relatively rapid release within a few hours to several days [20].

We also encapsulated cisplatin in SSRBCs using the classic hypotonic dialysis method. As shown in Fig. 7, for the PpIX concentration and light energy dose parameters employed, cisplatin efflux is 50% at 8 h, which is approximately 2-fold faster than that for calcein. Cisplatin's molecular weight is about half that of calcein; therefore it may escape through pores opened in the SSRBC membrane by photoactivation at a faster rate than calcein. Cisplatin's water solubility and neutral charge may also contribute to its rapid diffusibility [42]. The same measures used to adjust calcein efflux rate, such as modifying PpIX concentration and light energy dose, can be employed to regulate release of cisplatin and other drugs encapsulated in SSRBCs. For cisplatin specifically, the photo-oxidation rate of the drug-loaded SSRBCs may be slightly reduced by decreasing the PpIX concentration, the light energy dose (power and duration), and the temperature of the cells during photoactivation [22]. Efflux patterns for several other chemotherapeutic agents such as methotrexate [43], carboplatin [44], etoposide [45], fludarabine [46], bleomycin [47], and AraC [48] show 50% drug efflux ranging from minutes to several days after drug loading. For most of these drugs, the photo-oxidation conditions to produce delayed hemolysis release could be similar to those shown herein for calcein. Thus, the principles articulated here for encapsulation and photo-oxidation of release of calcein could be used to prepare cisplatin and a substantial number of other chemotherapeutic agents for delayed release in our system without undue experimentation.

As shown in this study, nRBCs do not release a significant amount of model drug in the tumor. Several anti-cancer agents have been encapsulated in nRBCs and used as drug carriers *in vivo* [49–53]. Such carriers, however, are rapidly engulfed and eliminated by the reticuloendothelial system [20,51,54]. Their failure to accumulate in tumors severely limits the ability of nRBCs to selectively deliver a drug payload to tumors. Liposomes and nanoparticles can localize to tumors through the enhanced permeability and retention (EPR) effect. Several such systems use near-infrared and ultraviolet light to release their contents [55–57]. For such cargo release *in vivo*, however, these systems rely on exogenous thermal or physical stimulus directed to tumors or tissue target site [6,38,39]. Such thermal/physical stimuli suffer the further drawback of inefficient tumor/tissue penetration [58]. In our system, by contrast, light activation is carried out *ex vivo* in a controlled environment prior to systemic administration and the drug-loaded SSRBCs do not require an exogenous tumor- or tissue-directed energy stimulus to release their contents. Moreover, unlike the other systems our drug-loaded SSRBCs should also be able to efficiently target metastatic as well as primary tumor sites without the aid of an external energy stimulus.

Since SSRBCs largely target hypoxic vasculature with upregulated adhesion receptors, cancer patients with vascular diseases bearing an underlying chronic oxidative stress signature [59] such as hypertension, atherosclerotic cardio- and cerebrovascular disease might be at additional risk. However, the risk of SSRBC treatment in these settings may be no greater than that of many widely used cancer cytotoxics (*e.g.*, doxorubicin), antiangiogenic agents (*e.g.*, bevacizumab), and biologics (*e.g.*, IL-2) which are known to exacerbate these very same vascular conditions. We previously reported that SSRBC infusions in tumor bearing mice showed a tumoricidal response with no significant constitutional toxicity or histologic evidence of tissue injury [2]. This evaluation also included histology of brain microvasculature which was devoid of inflammation, thrombosis, or necrosis. The lack of toxicity may be ascribed in part to the effectiveness of a single, small volume of SSRBCs (200 μL) administered to mice which translated to humans amounts to approximately 1 unit of packed red blood cells. Such a small volume of SSRBCs should preserve anti-tumor efficacy since it concentrates a large quantity of drug in the tumor vasculature.

With respect to the risk of alloimmunization, SSRBCs express the conventional ABO blood groups. In sickle cell patients who receive transfusions from normal donors, the prevalence of alloantibodies was 10% in those receiving fewer than 50 transfusions [60]. Alloimmunization to Rh C, D, E, and Kell was the most commonly encountered [61–66]. Extensive matching of donor and recipient red cell antigen phenotype significantly reduced the prevalence of alloantibodies [67]. In the current studies we used a small volume of photo-oxidized SSRBCs (200 μL) in

mice which when translated to humans amounts to approximately 1 unit of packed red blood cells. In our previous studies, a therapeutic effect was induced in mice with a single SSRBC infusion in the identical volume with no trace of hemolysis [2]. Thus, alloimmunization and transfusion reactions with our system could be minimized by using a single small volume infusion of SSRBCs coupled with careful screening of the SS cells for ABO, Rh C, D, E, and Kell antigens.

Collectively, these data show the feasibility of loading a model therapeutic into photosensitized SSRBCs which can then localize and accumulate in tumor microvasculature and release a 3–4 fold greater amount of drug into tumor tissue compared to normal tissue. Such an increased drug delivery to tumor by drug-loaded/photosensitized SSRBCs exceeds that by photosensitized nRBCs, non-photosensitized SSRBCs, and free drug in tumor tissue. Thus the drug-loaded/photosensitized SSRBCs appear to be a promising new strategy for selective drug delivery to hypoxic solid tumors notable for their resistance to existing cancer treatments.

Acknowledgments

The authors would like to thank Mark W. Dewhirst (Duke University, Durham, NC), Linda Jones (College of Charleston, Charleston, SC), and M-Ali H. Al-Akhras (Jordan University of Science and Technology, Irbid, Jordan) for insightful discussions, and Chul Han (University of Florida, Department of Physiology and Functional Genomics), and Yonghwan Kim (University of Florida, Department of Physiology and Functional Genomics) for technical support. This work was supported in part by a grant from the Bankhead–Coley Cancer Research Program, Florida Department of Health (to BSS), and the National Institutes of Health (NHLBI, 7K01HL103172 to AER).

References

[1] R.K. Jain, Delivery of molecular and cellular medicine to solid tumors, Adv. Drug Deliv. Rev. 46 (2001) 149–168.
[2] D.S. Terman, B.L. Viglianti, R. Zennadi, D. Fels, R.J. Boruta, H. Yuan, M.R. Dreher, G. Grant, Z.N. Rabbani, E. Moon, L. Lan, J. Eble, Y. Cao, B. Sorg, K. Ashcraft, G. Palmer, M.J. Telen, M.W. Dewhirst, Sickle erythrocytes target cytotoxics to hypoxic tumor microvessels and potentiate a tumoricidal response, PLoS One 8 (2013) e52543.
[3] D.S. Terman, Compositions and methods for treatment of neoplastic disease (2010), United States patent 7,803,637.
[4] E. Ruoslahti, Vascular zip codes in angiogenesis and metastasis, Biochem. Soc. Trans. 32 (2004) 397–402.
[5] M.A. Al-Akhras, L.I. Grossweiner, Sensitization of photohemolysis by hypericin and Photofrin, J. Photochem. Photobiol. B 34 (1996) 169–175.
[6] L.I. Grossweiner, J.M. Fernandez, M.D. Bilgin, Photosensitization of red blood cell haemolysis by photodynamic agents, Lasers Med. Sci. 13 (1998) 42–54.
[7] D.P. Valenzeno, Stoichiometry and creation of membrane lesions by hematoporphyrin derivative and light, IEEE J. Quantum Electron. 20 (1984) 1439–1441.
[8] J. Ieremia, C.A. Blau, Limitations of a mouse model of sickle cell anemia, Blood Cells Mol. Dis. 28 (2002) 146–151.
[9] C. Paszty, C.M. Brion, E. Manci, H.E. Witkowska, M.E. Stevens, N. Mohandas, E.M. Rubin, Transgenic knockout mice with exclusively human sickle hemoglobin and sickle cell disease, Science 278 (1997) 8876–8878.
[10] L.C. Wu, C.W. Sun, T.M. Ryan, K.M. Pawlik, J. Ren, T.M. Townes, Correction of sickle cell disease by homologous recombination in embryonic stem cells, Blood 108 (2006) 1183–1188.
[11] J. Hanna, M. Wernig, S. Markoulaki, C.W. Sun, A. Meissner, J.P. Cassady, C. Beard, T. Brambrink, L.C. Wu, T.M. Townes, R. Jaenisch, Treatment of sickle cell anemia mouse model with iPS cells generated from autologous skin, Science 318 (2007) 1920–1923.
[12] B.S. Sorg, M.E. Hardee, N. Agarwal, B.J. Moeller, M.W. Dewhirst, Spectral imaging facilitates visualization and measurements of unstable and abnormal microvascular oxygen transport in tumors, J. Biomed. Opt. 13 (2008), (article 014026).
[13] B.S. Sorg, B.J. Moeller, O. Donovan, Y. Cao, M.W. Dewhirst, Hyperspectral imaging of hemoglobin saturation in tumor microvasculature and tumor hypoxia development, J. Biomed. Opt. 10 (2005), (article 044004).
[14] J.L. Unthank, J.M. Lash, J.C. Nixon, R.A. Sidner, H.G. Bohlen, Evaluation of carbocyanine-labeled erythrocytes for microvascular measurements, Microvasc. Res. 45 (1993) 193–210.
[15] M.R. King, D. Bansal, M.B. Kim, I.H. Sarelius, The effect of hematocrit and leukocyte adherence on flow direction in the microcirculation, Ann. Biomed. Eng. 32 (2004) 803–814.
[16] S. Choe, A.P. Acharya, B.G. Keselowsky, B.S. Sorg, Intravital microscopy imaging of macrophage localization to immunogenic particles and co-localized tissue oxygen saturation, Acta Biomater. 6 (2010) 3491–3498.
[17] D.C. Turner, D. Moshkelani, C.S. Shemesh, D. Luc, H. Zhang, Near-infrared image-guided delivery and controlled release using optimized thermosensitive liposomes, Pharm. Res. 29 (2012) 2092–2103.
[18] Ž. Vanić, S. Barnert, R. Süss, R. Schubert, Fusogenic activity of PEGylated pH-sensitive liposomes, J. Liposome Res. 22 (2012) 148–157.
[19] M. Hamidi, N. Zarei, A. Zarrin, S. Mohammadi-Samani, Preparation and validation of carrier human erythrocytes loaded by bovine serum albumin as a model antigen/protein, Drug Deliv. 14 (2007) 295–300.
[20] M. Hamidi, H. Tajerzadeh, Carrier erythrocytes: an overview, Drug Deliv. 10 (2003) 9–20.
[21] M. Sooriyaarachchi, A. Narendranb, J. Gailer, Comparative hydrolysis and plasma protein binding of *cis*-platin and carboplatin in human plasma *in vitro*, Metallomics 3 (2011) 49–55.
[22] M. Al-Akhras, A new application of Gompertz function in photohemolysis: the effect of temperature on red blood cell hemolysis photosensitized by protoporphyrin IX, Med. Biol. Eng. Comput. 44 (2006) 703–710.
[23] E.A. Manci, C.A. Hillery, C.A. Bodian, Z.G. Zhang, G.A. Lutty, B.S. Coller, Pathology of Berkeley sickle cell mice: similarities and differences with human sickle cell disease, Blood 107 (2006) 1651–1658.
[24] J.P. Pooler, The kinetics of colloid osmotic hemolysis. II. Photohemolysis, Biochim. Biophys. Acta 812 (1985) 199–205.
[25] P.D. Patel, N. Dand, R.S. Hirlekar, V.J. Kadam, Drug loaded erythrocytes: as novel drug delivery system, Curr. Pharm. Des. 14 (2008) 63–70.
[26] V.S. Gopal, A.R. Kumar, A.N. Usha, A. Karthik, N. Udupa, Effective drug targeting by erythrocytes as carrier systems, Curr. Trends Biotechnol. Pharm. 1 (2007) 18–33.
[27] M.S. Newman, G.T. Colbern, P.K. Working, C. Engbers, M.A. Amantea, Comparative pharmacokinetics, tissue distribution, and therapeutic effectiveness of cisplatin encapsulated in long-circulating, pegylated liposomes (SPI-077) in tumor-bearing mice, Cancer Chemother. Pharmacol. 43 (1999) 1–7.
[28] W.C. Zamboni, A.C. Gervais, M.J. Egorin, J.H.M. Schellens, E.G. Zuhowski, D. Pluim, E. Joseph, D.R. Hamburger, P.K. Working, G. Colbern, M.E. Tonda, D.M. Potter, J.L. Eiseman, Systemic and tumor disposition of platinum after administration of cisplatin or STEALTH liposomal-cisplatin formulations (SPI-077 and SPI-077 B103) in a preclinical tumor model of melanoma, Cancer Chemother. Pharmacol. 53 (2004) 329–336.
[29] R.N. MacCallum, E.C. Lynch, J.D. Hellums, C.P. Alfrey, Fragility of abnormal erythrocytes evaluated by response to shear stress, J. Lab. Clin. Med. 85 (1975) 67–74.
[30] B.H. Rank, J. Carlsson, R.P. Hebbel, Abnormal redox status of membrane-protein thiols in sickle erythrocytes, J. Clin. Invest. 75 (1985) 1531–1537.
[31] S.K. Ballas, N. Mohandas, Sickle red cell microrheology and sickle blood rheology, Microcirculation 11 (2004) 209–225.
[32] G.A. Barabino, M.O. Platt, D.K. Kaul, Sickle cell biomechanics, Annu. Rev. Biomed. Eng. 12 (2010) 345–367.
[33] N. Conran, F.F. Costa, Hemoglobin disorders and endothelial cell interactions, Clin. Biochem. 42 (2009) 1824–1838.
[34] V. Koshkin, Correlation between multi-drug resistance-associated membrane transport in clonal cancer cells and the cell cycle phase, PLoS One 7 (2012) e1368.
[35] J. Asaumi, S. Kawasaki, M. Kuroda, Y. Takeda, K. Kishi, Y. Hiraki, Intracellular accumulation and retention of calcein in Ehrlich ascites tumor cells and their adriamycin-resistant strain, Anticancer. Res. 19 (1999) 4311–4314.
[36] B. Goldenbogen, N. Brodersen, A. Gramatica, M. Loew, J. Liebscher, A. Herrmann, H. Egger, B. Budde, A. Arbuzova, Reduction-sensitive liposomes from a multifunctional lipid conjugate and natural phospholipids: reduction and release kinetics and cellular uptake, Langmuir 27 (2011) 10820–10829.
[37] C.G. Millán, A.Z. Castañeda, M.L.S. Marinero, J.M. Lanao, Factors associated with the performance of carrier erythrocytes obtained by hypotonic dialysis, 33 (2004) 132–140.
[38] T. Ogiso, M. Iwaki, A. Ohtori, Encapsulation of dexamethasone in rabbit erythrocytes, the disposition in circulation and anti-inflammatory effect, J. Pharmacobiodyn 12 (1985) 1032–1040.
[39] L. Zolla, G. Lupidi, M. Marcheggiani, G. Falcioni, M. Brunori, Encapsulation of proteins into human erythrocytes: a kinetic investigation, Biochim. Biophys. Acta 1024 (1990) 5–9.
[40] A. Fazi, U. Mancini, E. Piatti, A. Accorsi, M. Magnani, Human red blood cells as bioreactors for the inactivation of harmful xenobiotics, Biotechnol. Appl. Biochem. 14 (1991) 60–68.
[41] C.G. Millán, M.L.S. Marinero, A.Z. Castañeda, J.M. Lanao, Drug, enzyme and peptide delivery using erythrocytes as carriers, J. Control. Release 95 (2004) 27–49.
[42] E. Reed, Cisplatin, carboplatin, and oxaliplatin, in: B.A. Chabner, D.L. Longo (Eds.), Cancer Chemotherapy and Biotherapy: Principles and Practice, Third edition, Lippincott Williams & Wilkins, Philadelphia, 2001, pp. 332–343.
[43] S.H. Yuan, W.H. Ge, J. Huo, X.H. Wang, Slow release properties and liver-targeting characteristics of methotrexate erythrocyte carriers, Fundam. Clin. Pharmacol. 23 (2009) 189–196.
[44] M. Tonetti, A. Gasparini, M. Giovine, D. Bini, A. Mazzucotelli, F. De Paz, U. Benatti, A. De Flora, Interaction of carboplatin with carrier human erythrocytes, Biotechnol. Appl. Biochem. 15 (1992) 267–277.
[45] L.A. Lotero, G. Olmos, J.C. Dıez, Delivery to macrophages and toxic action of etoposide carried in mouse red blood cells, Biochim. Biophys. Acta 17 (2003) 160–166.
[46] A. Fraternale, L. Rossi, M. Magnani, Encapsulation, metabolism and release of 2-fluoro-ara-AMP from human erythrocytes, Biochim. Biophys. Acta 1291 (1996) 149–154.

[47] W.E. Lynch, G.P. Sartiano, S.L. Rosenblum, J.H. Calkins, C.B. Ramsey, The use of erythrocytes for delivery of chemotherapeutic agents to the reticuloendothelial system, Bibl. Haematol. 51 (1985) 42–49.
[48] T. Kitao, K. Hattori, Erythrocyte entrapment of daunomycin by amphotericin B without hemolysis, Cancer Res. 40 (1980) 1351–1353.
[49] M. Magnani, L. Rossi, A. Fraternale, M. Bianchi, A. Antonelli, R. Crinellei, L. Chiarantini, Erythrocyte-mediated delivery of drugs, peptides and modified oligonucleotides, Gene Ther. 9 (2002) 749–751.
[50] Y. Godfrin, F. Horand, R. Franco, E. Dufour, E. Kosenko, B.E. Bax, A. Banz, O.A. Skorokhod, J.M. Lanao, V. Vitvitsky, E. Sinauridze, V. Bourgeaux, K.C. Gunter, International seminar on the red blood cells as vehicles for drugs, Expert. Opin. Biol. Ther. 12 (2012) 127–133.
[51] W.E. Lynch, G.P. Sartiano, A. Ghaffar, Erythrocytes as carriers of chemotherapeutic agents for targeting the reticuloendothelial system, Am. J. Hematol. 9 (1980) 249–259.
[52] A. De Flora, U. Benatti, L. Guida, E. Zocchi, Encapsulation of Adriamycin in human erythrocytes, Proc. Natl. Acad. Sci. U. S. A. 83 (1986) 7029–7033.
[53] O.A. Skorokhod, E.V. Kulikova, N.M. Galkina, P.V. Medvedev, E.E. Zybunova, V.M. Vitvitsky, A.V. Pivnik, F.I. Ataullakhanov, Doxorubicin pharmacokinetics in lymphoma patients treated with doxorubicin-loaded erythrocytes, Haematologica 92 (2007) 570–571.
[54] B.E. Bax, M.D. Bain, P.J. Talbot, E.J. Parker-Williams, R.A. Chalmers, Survival of human carrier erythrocytes *in vivo*, Clin. Sci. 96 (1999) 171–178.
[55] S. Carregal-Romero, M. Ochs, P. Rivera-Gil, C. Ganas, A.M. Pavlov, G.B. Sukhorukov, W.J. Parak, NIR-light triggered delivery of macromolecules into the cytosol, J. Control. Release 159 (2012) 120–127.
[56] L. Paasonen, T. Laaksonen, C. Johans, M. Yliperttula, K. Kontturi, A. Urtti, Gold nanoparticles enable selective light-induced contents release from liposomes, J. Control. Release 122 (2007) 86–93.
[57] D. Shi, M. Matsusaki, M. Akashi, Photo-tunable protein release from biodegradable nanoparticles composed of cinnamic acid derivatives, J. Control. Release 149 (2011) 182–189.
[58] T.L. Andresen, S.S. Jensen, K. Jørgensen, Advanced strategies in liposomal cancer therapy: problems and prospects of active and tumor specific drug release, Prog. Lipid Res. 44 (2005) 68–97.
[59] N.R. Madamanchi, A. Vendrov, M.S. Runge, Oxidative stress and vascular disease, Arterioscler. Thromb. Vasc. Biol. 25 (2005) 29–38.
[60] E.G. Reisner, D.D. Kostyu, G.J. Phillips, C. Walker, D.V. Dawson, Alloantibody responses in multiply transfused sickle cell patients, Tissue Antigens 30 (1987) 161–166.
[61] S.C. Davies, A.C. McWilliam, P.E. Hewitt, A. Devenish, M. Brozovic, Red cell alloimmunization in sickle cell disease, Br. J. Haematol. 63 (1986) 241–245.
[62] W.F. Rosse, D. Gallagher, T.R. Kinney, O. Castro, H. Dosik, J. Moohr, W. Wang, P.S. Levy, Transfusion and alloimmunization in sickle cell disease. The Cooperative Study of Sickle Cell Disease, Blood 76 (1990) 1431–1437.
[63] S. Sarnaik, J. Schornack, J.M. Lusher, The incidence of development of irregular red cell antibodies in patients with sickle cell anemia, Transfusion 26 (1986) 249–252.
[64] E. Vichinsky, Transfusion therapy, in: S.H. Embury, R.P. Hebbel, N. Mohandas, M.H. Steinberg (Eds.), Sickle Cell Disease: Basic Principles and Clinical Practice, Raven Press, New York, 1994, pp. 781–798.
[65] E.P. Vichinsky, E.A.R.A. Johnson, M.S. Hoag, A. Williams, B. Lubin, Alloimmunization in sickle cell anemia and transfusion of racially unmatched blood, N. Engl. J. Med. 322 (1990) 1617–1621.
[66] A.S. Wayne, S.V. Kevy, D.G. Nathan, Transfusion management of sickle cell disease, Blood 81 (1993) 1109–1123.
[67] D.R. Ambruso, J.H. Githens, R. Alcorn, D.J. Dixon, L.J. Brown, W.M. Vaughn, T. Hays, Experience with donors matched for minor blood group antigens in patients with sickle cell anemia who are receiving chronic transfusion therapy, Transfusion 27 (1987) 94–98.